Proc. Natl. Acad. Sci. USA
Vol. 86, pp. 1475–1479, March 1989
Biochemistry

Molecular structure of fructose-1,6-bisphosphatase at 2.8-Å resolution

(x-ray crystallography/allosteric enzyme/binding sites/fructose 2,6-bisphosphate/AMP)

HENGMING KE*, CHELESTE M. THORPE*, BARBARA A. SEATON*†, FRANK MARCUS‡§, AND WILLIAM N. LIPSCOMB*

*Gibbs Chemical Laboratory, Harvard University, 12 Oxford Street, Cambridge, MA 02138; and ‡Department of Biological Chemistry and Structure, University of Health Sciences/The Chicago Medical School, North Chicago, IL 60064

Contributed by William N. Lipscomb, December 1, 1988

ABSTRACT **Fructose-1,6-bisphosphatase (D-fructose-1,6-bisphosphate 1-phosphohydrolase, EC 3.1.3.11) from the cortex of pig kidney and its complexes with either fructose 2,6-bisphosphate (Fru-2,6-P_2) or adenosine monophosphate (AMP) have been crystallized in the space group $P3_221$. The three-dimensional structure of the native enzyme has been solved at 3.0-Å resolution by the multiple isomorphous replacement method and refined at 2.8-Å resolution to a crystallographic *R* factor of 0.194. A total of 316 of 335 residues, omitting disordered regions 1–5 and 54–67, have been built into the monomer, which has average dimensions of about 30 Å by 50 Å by 35 Å. Four monomeric units aggregate into a molecular tetramer with D_2 symmetry, which approximates a disk about 35 Å thick. Each monomer consists of about 33% α-helix, 23% β-strand, and 6% β-turn. Four sites for Fru-2,6-P_2 and two major sites for AMP binding per tetramer have been identified by difference Fourier techniques. The binding site for Fru-2,6-P_2 is shared by two neighboring monomers and consists of side-chain atoms of Asn-212, Tyr-244, Tyr-264, and Lys-274; backbone atoms of Gly-246 through Met-248; and only Arg-243 from the adjacent subunit. In addition, Asn-125, Tyr-215, and Lys-269 are located within a distance of about 5 Å of Fru-2,6-P_2. A negatively charged pocket near this binding site includes Asp-118, Asp-121, Glu-280, Glu-97, and Glu-98. The AMP binding site is located near Val-17, Gln-20, Gly-21, Ala-24 through Met-30, Lys-112, Tyr-113, Arg-140, and Met-177.**

Fructose-1,6-bisphosphatase (Fru-1,6-Pase; D-fructose-1,6-bisphosphate 1-phosphohydrolase, EC 3.1.3.11), a key regulatory enzyme in gluconeogenesis, catalyzes the hydrolysis of fructose 1,6-bisphosphate (Fru-1,6-P_2) to fructose 6-phosphate and inorganic phosphate. The catalytic and regulatory properties of the enzyme isolated from gluconeogenic tissues have been studied extensively (1–3). However, little is known about the three-dimensional structure of this tetrameric enzyme composed of four identical polypeptide chains. Seven complete amino acid sequences have been reported for pig kidney (4), sheep liver (5), yeast *Saccharomyces cerevisiae* (6), yeast *Schizosaccharomyces pombe* (6), *Escherichia coli* (7), wheat chloroplast (8), and rat liver (9) Fru-1,6-Pase. The activity of Fru-1,6-Pase is controlled by the action of two inhibitors, AMP and fructose 2,6-bisphosphate (Fru-2,6-P_2) and by alteration of mRNA supply (9). The inhibition by AMP is allosteric (10), but the mechanism of Fru-2,6-P_2 inhibition is unresolved. Contrasting views suggest Fru-2,6-P_2 binding to the active site, to an allosteric site, or to both (11, 12). Preliminary x-ray crystallographic studies have been reported on Fru-1,6-Pase crystals from chicken liver (13), turkey liver (14), rabbit liver (15), and pig kidney (16). Progress on collection of x-ray diffraction data from the rabbit liver enzyme has been reported (17).

We have grown crystals of native pig kidney Fru-1,6-Pase in the space group $P3_221$. In addition, crystals of its complexes with either Fru-2,6-P_2 or AMP have been grown in a form isomorphous to the native crystals. The three-dimensional structure of the native enzyme has been determined by the multiple isomorphous replacement (MIR) method. The binding sites for Fru-2,6-P_2 and AMP have been identified by difference Fourier techniques. Here, we report the general structural features of the enzyme; its secondary, tertiary, and quaternary structures; and the binding sites for Fru-2,6-P_2 and AMP. A more complete structure and the details of structure determination will be published elsewhere.

METHODS AND RESULTS

Pig kidney Fru-1,6-Pase was purified by using the modified method of Colombo and Marcus (18). Crystals of the native Fru-1,6-Pase were grown by dialyzing the enzyme solution (5–10 mg/ml) against a buffer containing 20 mM Tris base, 2.5 mM maleic acid, 0.1 mM EDTA, 0.3 mM NaN_3, and 4% (wt/vol) PEG at pH 7.4. Its complex with Fru-2,6-P_2 was crystallized by dialyzing the enzyme solution against the above buffer modified to contain 10 mM Tris base, 8% PEG, and 0.5 mM Fru-2,6-P_2. The AMP complex was prepared by using 10 mg of protein per ml, 20 mM cacodylate, 0.1 mM EDTA, 0.3 mM NaN_3, 12% PEG, and 1 mM AMP at pH 7.0. A 4-day dialysis produced crystals with a typical size of 0.4 × 0.4 × 0.7 mm in the shape of either a hexagonal bar or a diamond. The space group is $P3_221$ with unit cell dimensions of $a = b = 132.3$ and $c = 68.0$ Å, and two subunits exist in the crystallographic asymmetric unit.

Four heavy-atom derivatives were made by soaking the native crystals at pH 7.4 in a buffer containing 20 mM Tris base, 2.5 mM maleic acid, 15% PEG, and various heavy metals: 1 mM $K[Au(CN)_2]$ for 4 days, 0.5 mM UO_2Ac_2 for 4 days, 10 mM $TlNO_3$ for 6 days, 1 mM $TbCl_3$ for 8 days. The diffraction data of the native enzyme and its derivatives were collected at the Resource for Crystallography located in the laboratory of Nguyen huu Xuong at the University of California, San Diego. Two multiwire proportional chambers (Mark II or Mark III) (19) were used, and the Cu K_α radiation was monochromatized by a Ni filter. All data were collected to 2.8-Å resolution (Table 1), although the crystals of the derivatives and the AMP complex of the enzyme do not diffract well beyond 3.0-Å resolution.

The publication costs of this article were defrayed in part by page charge payment. This article must therefore be hereby marked "*advertisement*" in accordance with 18 U.S.C. §1734 solely to indicate this fact.

Abbreviations: Fru-1,6-Pase, fructose-1,6-bisphosphatase; Fru-2,6-P_2, fructose 2,6-bisphosphate; MIR, multiple isomorphous replacement.

†Present address: Department of Physiology, Boston University School of Medicine, 80 East Concord Street, Boston, MA 02118.
§Present address: Chiron Research Laboratories, Chiron Corporation, 4560 Horton Street, Emeryville, CA 94608-2916.

Heavy-atom positions for the four derivatives were located by the difference Patterson method and refined by the MIR method (20, 21). A molecular twofold axis relating the two subunits in the asymmetric unit was initially calculated from the heavy-atom positions and refined by the method of least squares (22). Most of the α-helices and β-sheets were recognizable in the MIR map at 3.0-Å resolution. This map was further improved by several methods: the modified procedure of Wang's solvent flattening (23), the averaging of density related by the molecular two-fold axis (24), and the combination of the averaged phases and the MIR phases (23, 25). All of the three maps showed significant improvements over the MIR map in terms of lower noise level, clearer molecular boundaries, and more recognizable side chains.

All of the electron density maps were calculated by a fast Fourier transformation program (26, 27). The F_o map calculated from the combined phases was used to trace the structure, while the other maps from the solvent flattening or the averaging or the MIR method were referred to for some ambiguous regions. The initial model for the native Fru-1,6-Pase structure was built by using the interactive computer program FRODO (28), which is linked to an Evans and Sutherland PS300, and refined by the program XPLOR (29) used with the CRAY XMP/48 at the Pittsburgh Supercomputing Center. After a five-stage simulated annealing procedure of the XPLOR refinement against 11,745 reflections at 3.0-Å resolution, the R factor dropped from 0.464 to 0.232. This refined structure was rebuilt and further refined against the 14,292 reflections between 8.0- and 2.8-Å resolution to an R factor of 0.194, where R is $\Sigma||F_o| - |F_c||/\Sigma|F_o|$. Solvent molecules have not yet been included in the refinement.

Difference Patterson maps for each derivative were calculated with the diffraction data between 15- and 3.8-Å resolution. The peaks of heavy atoms in the maps were strong and easily interpreted. To coordinate the origins for the different derivatives and for the different sites in each derivative, the phases from one site of the uranyl acetate derivative were used to locate the other three sites, and then these four sites were used to locate heavy-atom sites of the other derivatives. The MIR phases from the four derivatives were good enough to locate the binding sites of Fru-2,6-P_2 and AMP, although the averaged figure of merit was only 0.53. To obtain slightly better phases, the Fru-2,6-P_2 complex was artificially taken as an iodine derivative (Table 2), and the final averaged figure of merit increased to 0.56.

In the absence of anomalous scattering, the diffraction data do not differentiate between the space groups $P3_221$ and $P3_121$. Also, for each space group, the peaks in the difference Patterson map can be interpreted as the heavy-atom positions with either positive signs or negative signs due to the center of symmetry in the Patterson space. To resolve these ambiguities, the figures of merit for the normal data of the UO_2Ac_2 and $TbCl_3$ derivatives were calculated and compared. Two possibilities, the negative sites in $P3_121$ and the positive sites in $P3_221$, had obviously low figures of merit and were ruled out. To select the proper enantiomer, we used the anomalous scattering data of the uranate derivative in Wang's procedure, which showed faster convergence of the R factor in a few cycles of the flattening procedure for the correct enantiomer. Our final choice was the space group $P3_221$. This choice was confirmed by the presence of right-handed α-helices in the electron density.

Table 1. Summary of x-ray diffraction data on Fru-1,6-Pase and its derivatives in $P3_221$ form

Sample	Crystals, no.	Reflections, no. Total	Reflections, no. Unique	R factor,* %
Native	2	82,889	16,082	5.98
Complex†				
Fru-2,6-P_2	2	61,118	15,546	6.30
AMP	1	39,421	11,546	7.26
UO_2Ac_2	2	79,111	27,034‡	8.28
$TbCl_3$	2	67,636	15,384	10.54
$TlNO_3$	2	79,514	16,041	8.94
$K[Au(CN)_2]$	1	34,399	17,792	6.27

All of the data were collected to 2.8 Å.
*$R = \Sigma(|F|i - |F|j)/\Sigma(|F|i + |F|j)$, where $|F|i$ and $|F|j$ are the magnitude of reflections related by crystallographic symmetry.
†Complex of the enzyme with Fru-2,6-P_2 or AMP.
‡Bijvoet pairs were unmerged.

Table 2. Heavy atom parameters in space group $P3_221$

Site	x	y	z	Relative occupancy
$K[Au(CN)_2]$				
1	−0.1790	−0.3252	−0.0685	2.2
2	−0.3883	−0.4277	−0.2542	1.7
UO_2Ac_2				
1	−0.9689	−0.7484	−0.3121	2.4
2	−0.9286	−0.7444	−0.3027	1.4
3	−0.3067	−0.5204	−0.0625	2.0
4	−0.3128	−0.5273	−0.1525	1.6
$TlNO_3$				
1	−0.9345	−0.7317	−0.2982	1.9
2	−0.9042	−0.7055	−0.2850	1.2
3	−0.9690	−0.7525	−0.3059	1.1
4	−0.3061	−0.5245	−0.1454	1.9
5	−0.3044	−0.5203	−0.0767	1.6
$TbCl_3$				
1	−0.9587	−0.7421	−0.3101	3.2
2	−0.9258	−0.7315	−0.3015	2.8
3	−0.3099	−0.5221	−0.0631	2.9
4	−0.3097	−0.5263	−0.1396	2.1
Iodine*				
1	−0.4946	−0.2407	−0.7638	1.4
2	−0.4957	−0.2666	−0.7917	1.4
3	−0.3190	−0.2024	−0.6113	1.4
4	−0.3520	−0.2082	−0.5831	1.4

The temperature factors were set to 0.0 and not refined.
*Artificial derivative at the positions of Fru-2,6-P_2.

The pig kidney Fru-1,6-Pase amino acid sequence of Marcus *et al.* (4) has been used to trace the structure except for the replacements of Glu-156 by a glycine residue and Glu-228 by a glutamine residue, according to an updated sequence. In the initial stage, the noncrystallographic molecular twofold axis was marked in the map, and the density for one subunit was traced as four fragments of polyalanine, which corresponded to residues 10–53, 70–90, 130–230, and 248–335. To identify the correct sequential residues, aromatic side chains were locked into the density and then detailed tracing was initiated in both directions. The α-helix polarities in fragments 28–53 and 248–335 strongly indicated the direction of the polypeptide chain. These polarities and the recognizable aromatic side chains together greatly reduced possible ambiguities of tracing. Proline was also used as a chain marker because of its special shape and abundance in the enzyme. Even glycine was a good marker in well-resolved regions. Several alternative traces for each fragment were tried. If no serious violations occurred, a fragment of sequence longer than 20 residues was fixed. A serious violation can be defined as Van der Waals contacts shorter than 2.0 Å, a large percentage of hydrophobic residues having poor density, or a charged side chain closely interacting with hydrophobic groups. The four fragments were finally connected into two: one from Thr-1 through Ile-53 and another from Asp-74 through Ala-335, although the density in the region from Asp-74 through Cys-128 was not well resolved. Another subunit (polypeptide chain) in the asymmetric unit

was then generated by transforming the built subunit by using the molecular twofold axis.

This initial model was refined by the program XPLOR at 3.0-Å resolution to an *R* factor of 0.232. However, the map calculated from the refined model supplied no new information, possibly because of the limitation of the 3.0-Å resolution. The phases from the refined structure were further improved by averaging over noncrystallographic symmetry at 2.8-Å resolution. This averaged map showed much better resolution of density at the regions around Lys-109 and Asp-127 and indicated that the trace from Asp-74 through Cys-128 should be adjusted. The rebuilt model, including residues 6–53 and 68–335, was refined at 2.8-Å resolution to an *R* factor of 0.203. The last stage of model building included corrections of the configurations of some amino acids in the structure, and final refinement at 2.8-Å resolution yielded an *R* factor of 0.194 and the averaged root-mean-square deviations of 0.023 Å and 4.7° for the bond lengths and bond angles, respectively.

THE MOLECULAR STRUCTURE

No peak for a metal ion was found in the electron density map. The total of 316 residues that were traced aggregate into a single domain that has a hexahedral shape, with two parallel trapezoidal faces having an upper side of about 23 Å, a lower side of about 35 Å, and a height of about 50 Å. The thickness between the two trapezoids is about 35 Å. Two adjacent subunits in the asymmetric unit resemble a truncated pyramid. The other half of the tetramer interacts at the bottom of the truncated pyramids so that the whole molecule looks like a pseudohexagonal disk with a thickness of 35 Å. The tetramer has D_2 symmetry (Fig. 1).

One subunit consists of eight α-helices, 13 β-strands, and five β-turns, corresponding to a content of 33.4%, 23.0%, and 6.0%, respectively. The secondary structure is schematized in Fig. 2. The elements of the secondary structure are packed into five layers (Fig. 2 and Fig. 3). Helices of H1, H2, and H3 are parallel at the bottom of the pyramid, while a β-sheet of 8 strands stacks over the α-helices forming a second level so that the backbone orientation of the sheet is parallel to the axes of the α-helices. This sheet can be divided into two portions: the first half consists of B1–B4 (Cys-92 through Tyr-139) and is interrupted by two random coils (Fig. 2), while the second half consists of B5–B8 (Val-160 through Val-200) and shows a regular alternation of β-strands and β-turns. Most residues of the β-sheet in the second level are hydrophobic, and the helices at the first level orient their hydrophobic side chains toward this sheet to make favorable nonpolar interactions, thus forming a hydrophobic core. The third level is made up of two α-helices, H6 and H7 (Fig. 3). A proline residue in the middle of the helix H7 slightly distorts this helix. The fourth level is a β-sheet of 5 strands, a mixture of parallel and antiparallel strands from B9 through B13, which are parallel to the axes of the α-helices at the third level. Another hydrophobic core is formed by the interactions of the hydrophobic side chains from the helices in the third level and the strands in the fourth level. Finally, two α-helices, H5 and H8, cover the top of the truncated pyramid.

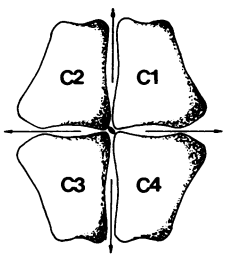

FIG. 1. A schematic diagram of Fru-1,6-Pase looking down a molecular twofold axis. In the plane of the drawing, the vertical twofold axis is the noncrystallographic molecular twofold axis, while the horizontal one is the crystallographic twofold axis. Subunits C1 and C2 make up the crystallographically asymmetric unit.

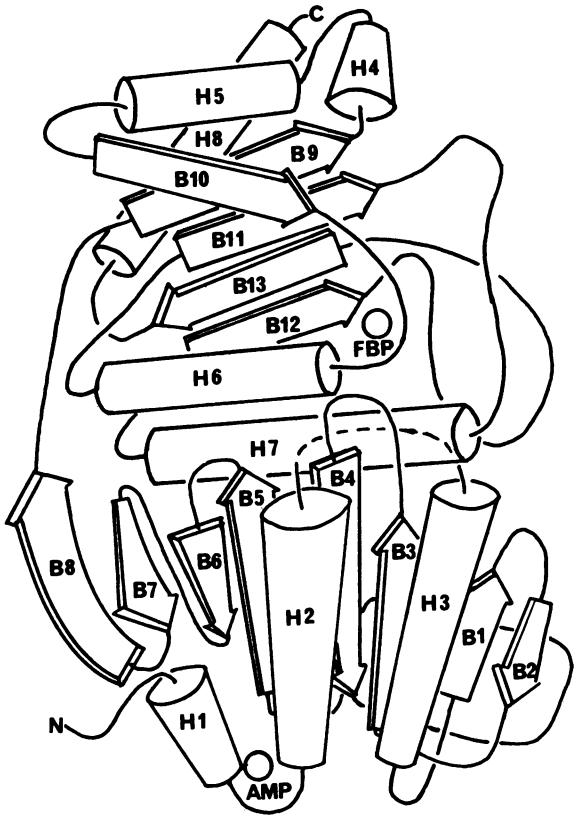

FIG. 2. Secondary structure of one subunit (C1) of Fru-1,6-Pase. The letters N and C represent the N and C termini, respectively. The α-helices are shown as cylinders, and the β-strands, as arrows. The dotted line between H2 and H3 represents the missing loop of Ala-54 through Gly-67. Two circles labeled FBP and AMP indicate the binding locations of Fru-2,6-P_2 and AMP, respectively. A rotation of about 50° around a horizontal axis and then a rotation of 90° around the new vertical axis transforms the drawing to the same view as Fig. 1. In the sequence of the chloroplast Fru-1,6-Pase (8), there is an extra fragment between residues 140 and 150, which can be placed at the molecular surface around the loop containing residue 147 in our structure.

DISCUSSION

In the difference Fourier map between the native enzyme and its Fru-2,6-P_2 complex, there are two approximately equal strongest peaks (more than 6 times the background average) in the crystallographic asymmetric unit, suggesting that Fru-2,6-P_2 binds at one site per subunit under those conditions of crystallization. The binding site (Fig. 3 and Fig. 4) has a shape of an oval cave with dimensions of about 18 × 12 Å and about 10 Å deep. Residues very near or interacting with Fru-2,6-P_2 are: side-chain atoms of Asn-212, Tyr-244, Tyr-264, and Lys-274; backbone atoms of Gly-246 through Met-248 from one subunit; and only Arg 243 from the neighboring chain. In addition, Asn-125, Tyr-215, and Lys-269 are fairly close to Fru-2,6-P_2, within a distance of about 5 Å. A negatively charged pocket makes up one wall of the binding site of Fru-2,6-P_2 and contains residues Asp-118, Asp-121, and Glu-280. In addition, hydrogen bonds between Glu-97 and Arg-276 and between Glu-98 and Lys-71 form an edge of the cave near the negatively charged pocket. The configuration of Fru-2,6-P_2 and the detailed interactions between Fru-2,6-P_2 and the enzyme will be published elsewhere.

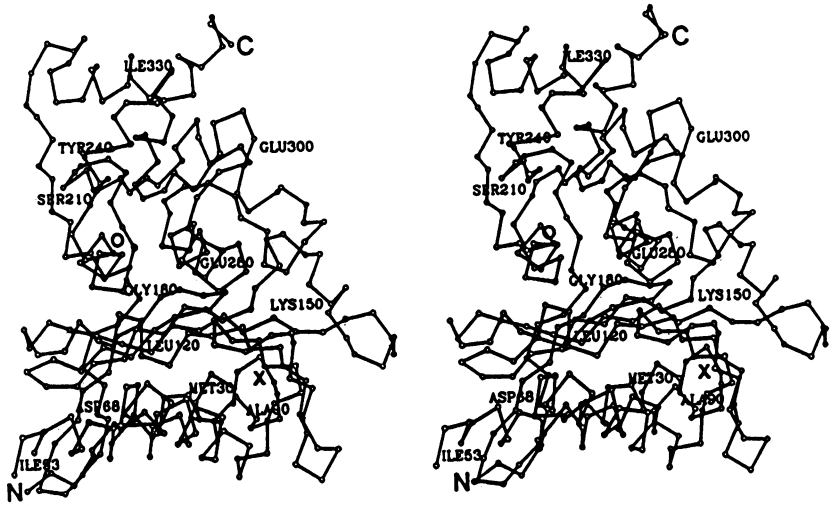

FIG. 3. A stereo plot of α-carbon atoms in one subunit (C1) with the same view as Fig. 1. The Fru-2,6-P_2 binding site is shown as a big circle, and the AMP site, as an X. The N and C termini are represented by letters N and C. The three twofold axes are almost horizontal, vertical, and perpendicular to the paper. The first residue shown in the N-terminal region is Phe-6 because the first five are disordered. Between Ile-53 and Asp-68 there are 14 residues missing from our map because of disorder or proteolytic cleavage.

Inspection of the primary sequences of the seven published Fru-1,6-Pases (4–9) reveals that 14 of the above 18 residues are conserved in comparison with the sequence homologies of only about 47% among the mammalian and yeast enzymes (6) and only about 45% among the mammalian and chloroplast enzymes (8). In fact, all of the residues that are directly interacting with Fru-2,6-P_2 or located at the negatively charged pocket are conserved, including Lys-274, a residue presumed from chemical modification data to be located at the active site of Fru-1,6-Pase (4). Conservation of the above residues also extends to the sequence of spinach leaf chloroplast Fru-1,6-Pase (F.M., unpublished results), a fact that strongly suggests that binding of Fru-2,6-P_2 occurs at the active site (30). Although the mechanism of inhibition of Fru-1,6-Pase by Fru-2,6-P_2 is controversial, with views in favor of Fru-2,6-P_2 binding to the active site (30–35), to a distinct allosteric site (36–38), or to both (39, 40), most workers in the field favor the idea of Fru-2,6-P_2 binding to the enzyme's active site. The present results indicate that binding of Fru-2,6-P_2 at two distinct sites, the catalytic site and an allosteric site (39), is unlikely because only one site per subunit was found in our difference Fourier map and also in the binding studies (34, 41). Another hypothesis suggests that Fru-2,6-P_2 could interact perhaps with both catalytic-site residues and allosteric-site residues (40); however, our model reveals a distance of more than 30 Å between the Fru-2,6-P_2 and AMP sites. This distance excludes simultaneous interaction of Fru-2,6-P_2 at both sites.

We suggest that Fru-2,6-P_2 binds to the active site and that the negatively charged pocket is an ideal site for a catalytic metal ion (2). Moreover, a magnesium ion interacting with both the negatively charged pocket and a phosphate group of Fru-2,6-P_2 has been identified in the difference Fourier map between the native enzyme and its cocrystal with magnesium, a result that we shall report elsewhere.

Two major sites per tetramer for the binding of AMP have been identified in the difference Fourier map between the native enzyme and its AMP complex. Some density was visible at the position related by the molecular twofold axis and was about 30% as strong as its noncrystallographically related mate. Kinetically, the bovine liver enzyme appeared to show two sites for AMP binding (42), but two additional sites were observed when the concentration of AMP was raised to 0.2 mM (43). This result is consistent with our crystallographic study. However, we cannot rule out a crystallographic influence on the unequal binding of AMP at the two pairs of sites per tetramer. The major AMP site interacts with Asn-142 from an adjacent tetramer in the crystal, while the minor site does not. Four sites for AMP binding per tetramer were reported (41, 44), but the saturation of these sites is more readily achieved in the presence of the substrate (45).

Our preliminary data suggest that AMP is near backbone and side-chain atoms of residues Val-17, Gln-20, Gly-21, and Ala-24 through Met-30, while residues Lys-112, Tyr-113, Arg-140, and Met-177 present nearby side chains (Fig. 5). Based on this binding geometry, it is not surprising that the so-called alkaline form of the enzyme, which is "nicked" at or near residue 60, shows decreased AMP binding and inhibition (1). Furthermore, the removal of residues 1–25 of pig kidney Fru-1,6-Pase results in the formation of an active AMP-insensitive enzyme (46). The UV difference spectrum of Fru-1,6-Pase induced by AMP showed two maxima at 288 and 279 nm that were interpreted as perturbations in the environment of tyrosine residues (40). Our structure suggests that this UV change may be contributed from Tyr-113, which is conserved throughout all known sequences.

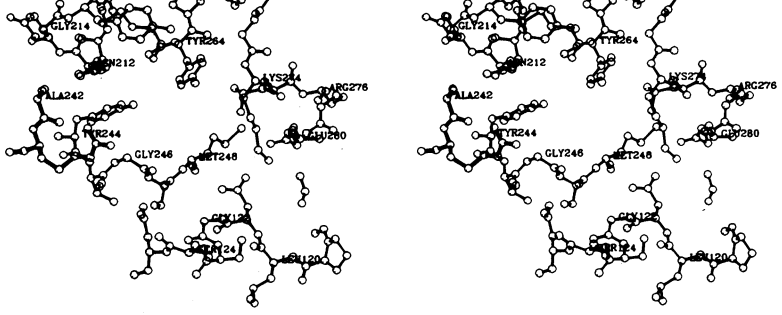

FIG. 4. A stereo view of the Fru-2,6-P_2 binding site. The lighter lines represent the residues from subunit C1, while the darker lines represent the residues from the next subunit (C2). The orientation of the plot is the same as that in Fig. 3.

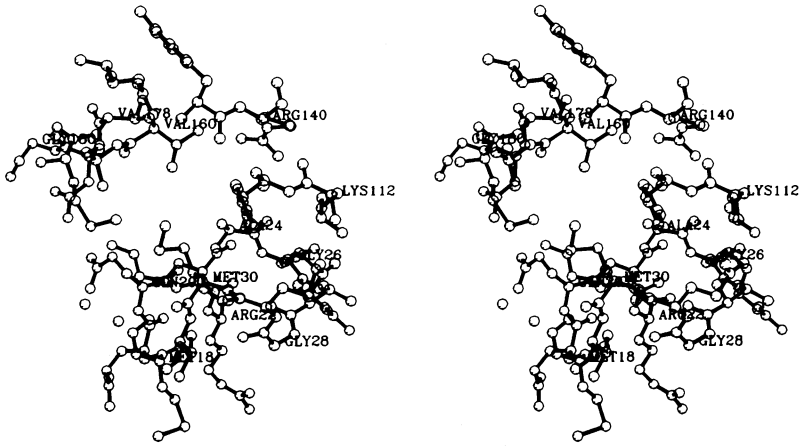

FIG. 5. A stereo view of the AMP binding site looking down the same direction as in Fig. 1.

In our structure, 19 residues are omitted because of lack of density, including the first 5 residues and the loop of Ala-54 through Gly-67. Extrapolation from the traceable density places the loop of Ala-54 through Gly-67 at the surface of the molecule interacting with the N terminus of the neighboring subunit. This loop has been identified as a proteolytically sensitive region in all Fru-1,6-Pases (47) and therefore may exist in multiple conformations, may be disordered at the resolution of our study, or even may not exist because of proteolytic cleavage.

J. E. Gouaux is acknowledged for his generous help with the refinement. We thank the National Institutes of Health for Grant GM06920 (to W.N.L.) and DK 21167 (to F.M.) and the Pittsburgh Supercomputing Center and National Science Foundation for support of the computing facilities. We also thank Dr. N. h. Xuong for use of the data collection Resource for Crystallography at University of California, San Diego (Grant RR01644). B. A. Seaton was supported by the American Cancer Society Postdoctoral Fellowship PF-2410.

1. Marcus, F. (1981) in *The Regulation of Carbohydrate Formation and Utilization in Mammals*, ed. Veneziale, C. M. (University Park Press, Baltimore), pp. 269–290.
2. Benkovic, S. J. & deMaine, M. M. (1982) *Adv. Enzymol.* **53**, 45–82.
3. Tejwani, G. A. (1983) *Adv. Enzymol.* **54**, 121–194.
4. Marcus, F., Edelstein, I., Reardon, I. & Heinrikson, R. L. (1982) *Proc. Natl. Acad. Sci. USA* **79**, 7161–7165.
5. Fisher, W. K. & Thompson, E. O. P. (1983) *Aust. J. Biol. Sci.* **36**, 235–250.
6. Rogers, D. T., Hiller, E., Mitsock, L. & Orr, E. (1988) *J. Biol. Chem.* **263**, 6051–6057.
7. Hamilton, W. D. O., Harrison, D. A. & Dyer, T. A. (1988) *Nucleic Acids Res.* **16**, 8707.
8. Raines, C. A., Lloyd, J. C., Longstaff, M., Bradley, D. & Dyer, T. (1988) *Nucleic Acids Res.* **16**, 7931–7942.
9. El-Maghrabi, M. R., Pilkis, J., Marker, A. J., Colosia, A. D., D'Angelo, G., Fraser, B. A. & Pilkis, S. J. (1988) *Proc. Natl. Acad. Sci. USA* **85**, 8430–8434.
10. Taketa, K. & Pogell, B. M. (1965) *J. Biol. Chem.* **240**, 651–662.
11. Pilkis, S. J., Claus, T. H., Kountz, P. D. & El-Maghrabi, M. R. (1987) *The Enzymes* (Academic, New York), Vol. 18, 3rd Ed., pp. 3–46.
12. Van Schaftingen, E. (1987) *Adv. Enzymol.* **59**, 315–395.
13. Anderson, W. F. & Matthews, B. W. (1977) *J. Biol. Chem.* **252**, 5556–5557.
14. McPherson, A., Burkey, D. & Stankiewicz, P. (1977) *J. Biol. Chem.* **252**, 7031–7034.
15. Soloway, B. & McPherson, A. (1978) *J. Biol. Chem.* **253**, 2461–2462.
16. Seaton, B. A., Campbell, R. L., Petsko, G. A., Rose, D. R., Edelstein, I. & Marcus, F. (1984) *J. Biol. Chem.* **259**, 8915–8916.
17. Weeks, C. M., Erman, M. & Ghosh, D. (1988) Abstracts, *Annual Meeting of American Crystallographic Association* (Philadelphia, PA, June 26–July 1, 1988), p. 69.
18. Colombo, G. & Marcus, F. (1973) *J. Biol. Chem.* **248**, 4923–4925.
19. Hamlin, R., Cork, C., Howard, A., Nielson, C., Vernon, W., Mathews, D. & Xuong, N. h. (1981) *J. Appl. Crystallogr.* **14**, 85–93.
20. Dickerson, R. E., Kendrew, J. C. & Strandberg, B. E. (1961) *Acta Crystallogr.* **14**, 1188–1195.
21. Terwilliger, T. C. & Eisenberg, D. (1983) *Acta Crystallogr. Sect. A* **39**, 813–817.
22. Cox, J. M. (1967) *J. Mol. Biol.* **28**, 151–156.
23. Wang, B. C. (1985) *Methods Enzymol.* **115**, 90–112.
24. Bricogne, G. (1976) *Acta Crystallogr. Sect. A* **32**, 832–847.
25. Hendrickson, W. A. & Lattman, E. E. (1970) *Acta Crystallogr. Sect. B* **26**, 136–143.
26. Ten Eyck, L. F. (1973) *Acta Crystallogr. Sect. A* **29**, 182–191.
27. Ten Eyck, L. F. (1977) *Acta Crystallogr. Sect. A* **33**, 486–492.
28. Jones, T. A. (1982) in *Computational Crystallography*, ed. Sayer, D. (Oxford Univ. Press, London), pp. 303–317.
29. Brünger, A. T., Kuriyan, J. & Karplus, M. (1987) *Science* **235**, 458–460.
30. Gottschalk, M. E., Chatterjee, T., Edelstein, I. & Marcus, F. (1982) *J. Biol. Chem.* **257**, 8016–8020.
31. Pilkis, S. J., El-Maghrabi, M. R., Pilkis, J. & Claus, T. H. (1981) *J. Biol. Chem.* **256**, 3619–3622.
32. Pontremoli, S., Melloni, E., Michetti, M., Salamino, F., Sparatore, B. & Horecker, B. L. (1982) *Arch. Biochem. Biophys.* **218**, 609–613.
33. Ganson, N. J. & Fromm, H. J. (1982) *Biochem. Biophys. Res. Commun.* **108**, 233–239.
34. Kitajima, S. & Uyeda, K. (1983) *J. Biol. Chem.* **258**, 7352–7357.
35. Liu, F. & Fromm, H. J. (1988) *J. Biol. Chem.* **263**, 10035–10039.
36. Van Schaftingen, E. & Hers, H. G. (1981) *Proc. Natl. Acad. Sci. USA* **78**, 2861–2863.
37. Francis, J., Van Schaftingen, E. & Hers, H. G. (1983) *Eur. J. Biochem.* **134**, 269–273.
38. Reyes, A., Hubert, E. & Slebe, J. C. (1985) *Biochem. Biophys. Res. Commun.* **127**, 373–379.
39. Meek, D. W. & Nimmo, H. G. (1983) *FEBS Lett.* **160**, 105–109.
40. Pilkis, S. J., El-Maghrabi, M. R., McGrane, M. M., Pilkis, J. & Claus, T. H. (1981) *J. Biol. Chem.* **256**, 11489–11495.
41. McGrane, M. M., El-Maghrabi, M. R. & Pilkis, S. J. (1983) *J. Biol. Chem.* **258**, 10445–10454.
42. Nimmo, H. G. & Tipton, K. F. (1975) *Eur. J. Biochem.* **58**, 575–585.
43. Arneson, R. M., Geller, A. M. & Byene, W. L. (1979) *Enzyme* **24**, 132–136.
44. Kratowich, N. & Mendicino, J. (1974) *J. Biol. Chem.* **249**, 5485–5494.
45. Sarngadharan, M. G., Watanabe, A. & Pogell, B. M. (1969) *Biochemistry* **8**, 1411–1419.
46. Chatterjee, T., Reardon, I., Heinrikson, R. L. & Marcus, F. (1985) *J. Biol. Chem.* **160**, 13553–13559.
47. Marcus, F., Harrsch, P. B., Moberly, L., Edelstein, I. & Latshaw, S. P. (1987) *Biochemistry* **26**, 7029–7035.